Human Molecular Genetics, 2010, Vol. 19, No. 5 ***837–847***
doi:10.1093/hmg/ddp552
Advance Access published on December 10, 2009

Conditional Niemann-Pick C mice demonstrate cell autonomous Purkinje cell neurodegeneration

Matthew J. Elrick[1,2,3], Chris D. Pacheco[1,2], Ting Yu[1], Nahid Dadgar[1], Vikram G. Shakkottai[4], Christopher Ware[1], Henry L. Paulson[4] and Andrew P. Lieberman[1,2,*]

[1]Department of Pathology, [2]Neuroscience Program, [3]Medical Scientist Training Program and [4]Department of Neurology, University of Michigan, Ann Arbor, MI 48109, USA

Received November 3, 2009; Revised and Accepted December 8, 2009

Pathways regulating neuronal vulnerability are poorly understood, yet are central to identifying therapeutic targets for degenerative neurological diseases. Here, we characterize mechanisms underlying neurodegeneration in Niemann-Pick type C (NPC) disease, a lysosomal storage disorder characterized by impaired cholesterol trafficking. To date, the relative contributions of neuronal and glial defects to neuron loss are poorly defined. Using gene targeting, we generate Npc1 conditional null mutant mice. Deletion of *Npc1* in mature cerebellar Purkinje cells leads to an age-dependent impairment in motor tasks, including rotarod and balance beam performance. Surprisingly, these mice did not show the early death or weight loss that are characteristic of global *Npc1* null mice, suggesting that Purkinje cell degeneration does not underlie these phenotypes. Histological examination revealed the progressive loss of Purkinje cells in an anterior-to-posterior gradient. This cell autonomous neurodegeneration occurs in a spatiotemporal pattern similar to that of global knockout mice. A subpopulation of Purkinje cells in the posterior cerebellum exhibits marked resistance to cell death despite Npc1 deletion. To explore this selective response, we investigated the electrophysiological properties of vulnerable and susceptible Purkinje cell subpopulations. Unexpectedly, Purkinje cells in both subpopulations displayed no electrophysiological abnormalities prior to degeneration. Our data establish that Npc1 deficiency leads to cell autonomous, selective neurodegeneration and suggest that the ataxic symptoms of NPC disease arise from Purkinje cell death rather than cellular dysfunction.

INTRODUCTION

Niemann-Pick type C (NPC) disease is an autosomal recessive neurovisceral lipid storage disorder of childhood, characterized by liver dysfunction and neurodegeneration resulting in progressive cognitive impairment, ataxia, seizures, dystonia and early mortality (1). NPC disease is caused by loss-of-function mutations in the *NPC1* or *NPC2* genes, members of an intracellular lipid trafficking pathway that act cooperatively to facilitate the efflux of exogenously derived cholesterol from endosomes and lysosomes (2–4). As a result of these mutations, intracellular lipid trafficking is deficient and unesterified cholesterol and glycosphingolipids accumulate in late endosomes and lysosomes (5). Currently, the link between lipid storage and the neurodegeneration that mediates patient mortality is unknown, and the mechanisms leading to selective neuronal vulnerability in NPC disease are not understood.

From studies of animal models of NPC, including mice in which an insertional mutation disrupts the *Npc1* gene (6), several general principles have emerged that guide our understanding of disease pathogenesis (7). In Npc1 deficient mice, as in patients with this disorder, neurons accumulate lipids, abnormally swollen axons are frequent and demyelination is present (8). These features are associated with impaired motor function and early death that model the degenerative phenotype of patients with this disease (9). Although systemic manifestations also occur in both NPC disease patients and mice, progressive neurological impairment is due to loss of functional Npc1 protein in the nervous system (10).

*To whom correspondence should be addressed at: Department of Pathology, University of Michigan Medical School, 3510 MSRB1, 1150 W. Medical Center Dr., Ann Arbor, MI 48109-0605, USA. Tel: +1 7346474624; Fax: +1 73461534441; Email: liebermn@umich.edu

Neurotoxicity is associated with the appearance of abnormal dendrites (11), the accumulation of hyperphosphorylated tau (12,13), a dysregulation of lysosomal calcium homeostasis (14) and the activation of autophagy (15,16), thereby implicating a host of mechanisms that may act as mediators of neuronal dysfunction or serve as compensatory responses elicited to promote neuronal survival. Many of these pathways are predicted to act within neurons to influence cell survival, consistent with an analysis of chimeric mice that suggested Npc1 deficiency triggers cell autonomous Purkinje cell loss (15). In contrast, transgenic rescue experiments in NPC mouse and drosophila models (17,18), and co-culture experiments with neurons and astrocytes (19), indicate that glia are critical contributors to neurotoxicity and question the extent to which neuronal loss is cell autonomous.

Our understanding of disease mechanisms is also guided by recent therapeutic insights from studies of NPC mice. Most striking are data demonstrating that a single dose of the neurosteroid allopregnanolone delivered with cyclodextrin (20) or cyclodextrin alone (21) at postnatal day 7 ameliorates Purkinje cell loss and motor deficits while prolonging overall survival. In contrast, similar intervention at postnatal weeks 2–3 has significantly diminished affects (20). These data raise the possibility that there exists a critical period for Purkinje cell loss in Npc1 deficient mice during development or early postnatal life. This notion, however, has not been rigorously tested.

To resolve these questions, we generated a conditional null mutant of the mouse *Npc1* gene, and used it to study effects of Purkinje cell-specific gene deletion. Of all neuronal populations affected by NPC disease, Purkinje cells degenerate earliest and to the greatest extent (5). As the sole output of the cerebellar cortex, their loss is thought to underlie the ataxic symptoms of NPC patients. In NPC mice, Purkinje cell loss progresses through a well-characterized anterior-to-posterior gradient, with the majority of Purkinje cells lost by end stage (22). Here, we demonstrate that cell-specific deletion of *Npc1* in Purkinje cells at postnatal weeks 2–3 is sufficient to cause Purkinje cell degeneration in a spatiotemporal pattern similar to that seen in global null mice, thus demonstrating cell autonomous neuronal loss that is independent of effects during embryonic development or the first postnatal week. Further, we show that a subpopulation of Purkinje cells in the posterior cerebellum survives despite *Npc1* deletion. Finally, we investigate the electrophysiologic properties of degenerating Purkinje cells and show that electrophysiological dysfunction does not precede Purkinje cell death.

RESULTS

Generation and characterization of $Npc1^{flox}$ mice

To generate a conditional null mutant of the mouse *Npc1* gene ($Npc1^{flox}$ mice), we used gene targeting to insert *lox*P sites on either side of exon 9 (Fig. 1A). Cre-mediated excision of exon 9 is predicted to cause the splicing of exon 8 directly to exon 10, leading to a frameshift and the incorporation of multiple stop codons. This strategy was chosen since an analogous spontaneous mutation is found in the widely used npc^{nih} ($Npc1^{-/-}$) mouse, in which a retrotransposon insertion into exon 9 introduces multiple stop codons (6) and yields a functional null allele.

Following production of $Npc1^{flox}$ mice (Fig. 1B and C), we verified that the targeted allele produces normal amounts of Npc1 protein, and that Cre-mediated deletion of exon 9 yields a functional null that is equivalent to the $Npc1^{-}$ allele of npc^{nih} mice. To delete the floxed allele in the germline, we used mice expressing Cre recombinase under the control of the ubiquitous EIIa promoter (23). The resulting mosaic offspring were bred with $Npc1^{+/-}$ mice to generate $Npc1^{\Delta/-}$ compound heterozygotes, where Δ indicates the germline-deleted version of the floxed Npc1 allele. Similar to $Npc1^{-/-}$ mice, $Npc1^{\Delta/-}$ compound heterozygotes expressed no detectable Npc1 protein (Fig. 1D) and decreased amounts of *Npc1* mRNA (Fig. 1E). In contrast, $Npc1^{flox/flox}$ mice expressed wild-type levels of Npc1 protein and slightly elevated levels of *Npc1* mRNA.

The functional consequences of germline deletion of the floxed allele were weight loss, motor deficits and premature death, similar to the phenotype of $Npc1^{-/-}$ mice (9,24). $Npc1^{\Delta/-}$ mice, but not $Npc1^{flox/-}$ controls, showed small size at weaning, followed by weight loss initiating at $\sim$7 weeks (Fig. 2A and B), impaired rotarod performance (Fig. 2C) and early death at an average of 48.1 ± 5.1 days (Fig. 2D). This phenotype was verified on a second, independently derived line of gene targeted mice (data not shown). Although this time course of disease is more accelerated than what is typically reported for $Npc1^{-/-}$ mice on the *Balb/c* background (9), we observed a similarly severe phenotype in $Npc1^{-/-}$ mice backcrossed ten generations onto C57BL6/J (data not shown). This finding is consistent with a prior report demonstrating the influence of strain background on the severity of the phenotype of $Npc1^{-/-}$ mice (25). Pathological examination of cerebellar tissue demonstrated Purkinje cell loss by 7 weeks (Fig. 2E). This was associated with marked microgliosis and astrogliosis throughout the brain, and the proliferation of foamy macrophages in the liver (Supplementary Material, Fig. S1), all of which are prominent features of NPC disease and are identical to the pathology of $Npc1^{-/-}$ mice. Furthermore, staining with filipin identified accumulations of unesterified cholesterol in $Npc1^{\Delta/-}$ and $Npc1^{-/-}$ mice, but not in $Npc1^{flox/-}$ controls (Fig. 2E). We conclude that *in vivo* deletion of $Npc1^{flox}$ inactivates the *Npc1* gene and reproduces the NPC phenotype.

Purkinje cell specific deletion of *Npc1* causes ataxia, but not weight loss or early mortality

We next sought to determine the extent to which cell autonomous toxicity mediates Purkinje cell loss in Npc1 deficient mice. To achieve Purkinje cell specific deletion of *Npc1*, we used *Pcp2-Cre* mice (26), in which expression of Cre recombinase is limited to cerebellar Purkinje cells and retinal bipolar neurons. Expression in Purkinje cells is initiated when these neurons acquire their adult pattern of gene expression, beginning as early as postnatal day 6 in some cells, and present in all Purkinje cells by postnatal weeks 2–3. Deletion of *Npc1* by this strategy is therefore not only cell-type restricted, but also post-developmental. Purkinje cell specific null mutants ($Npc1^{flox/-}$;*Pcp2-Cre*$^{+}$), but not littermate controls ($Npc1^{flox/+}$;*Pcp2-Cre*$^{+}$), displayed age-dependent motor deficits detectable by impaired rotarod performance by 15 weeks (Fig. 3A), decreased ability to traverse a balance beam by 10 weeks (Fig. 3B) and tremors by 13 weeks (data not shown).

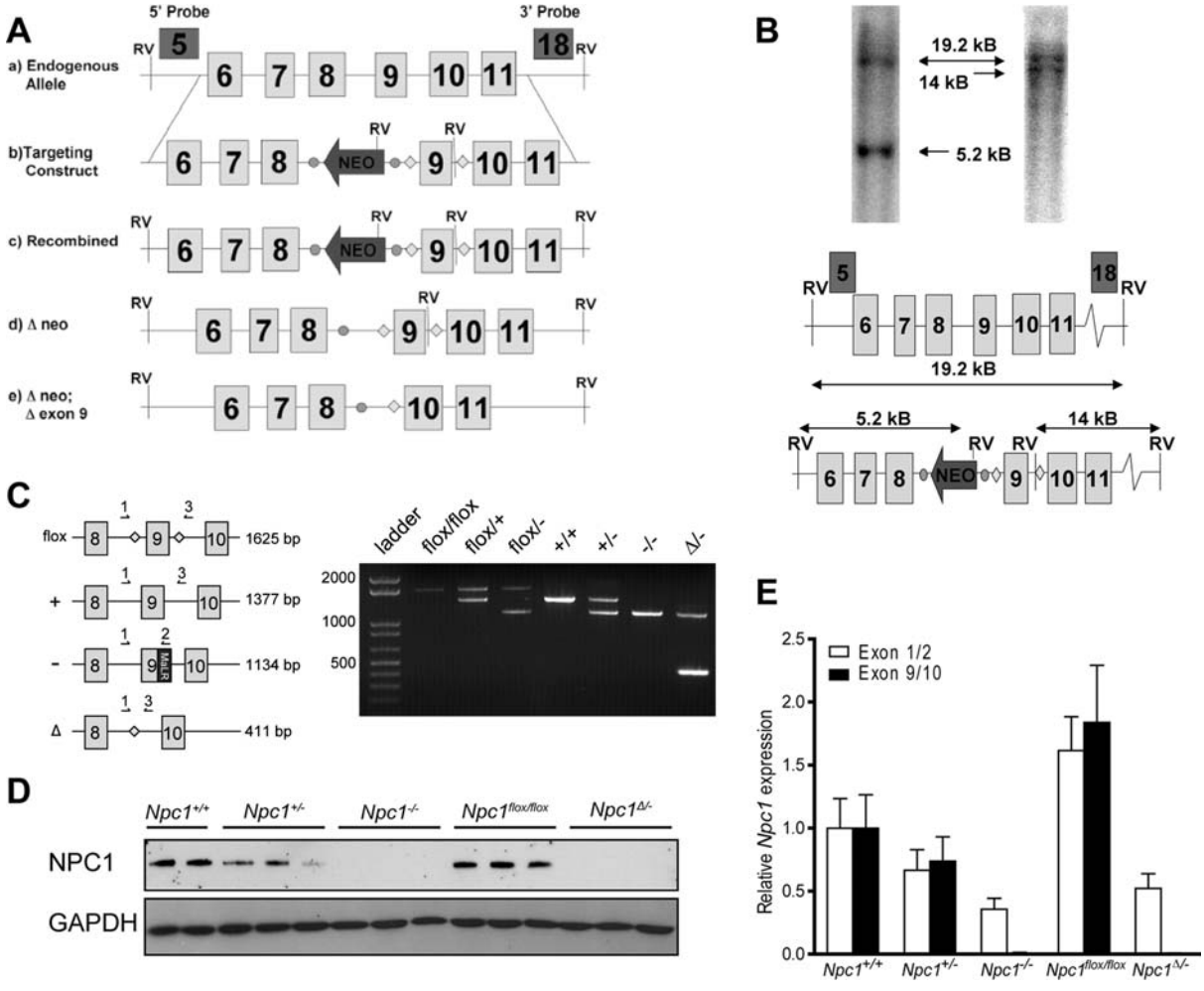

Figure 1. Generation of *Npc1*^{flox} mice. (**A**) Schematic representation of the endogenous *Npc1* locus (a), targeting construct (b), locus following homologous recombination (c), FLP-mediated deletion of the neomycin resistance cassette (d) and Cre-mediated deletion of exon 9. FRT sites are shown as circles, *lox*P sites are represented by diamonds. (**B**) Genomic Southern blot of tail biopsy derived DNA from a black pup sired by one of two independently derived male chimeras. Genomic DNA was digested with *Eco*RV and Southern blots analyzed using probes that fall outside the targeting vector. The 5′ exon 5 (on left) and 3′ exon 18 (on right) probes both hybridize to a 19.2 kb band from the non-recombined allele. The recombined *Npc1* allele generates a 5.2 kb band with the 5' probe and a 14 kb band with the 3′ probe. (**C**) PCR genotyping of *Npc1* mutant mice. Left panel: Schematic representation of primers used. Right panel: PCR products visualized by agarose gel electrophoresis. (**D**) Western blot for NPC1 protein in mouse liver lysates. (**E**) Quantitative RT–PCR for *Npc1* mRNA as detected by probes recognizing the junction between exons 1 and 2 (white bars) or exons 9 and 10 (black bars). $N = 3$ mice per genotype. Data are mean ± SEM.

However, Purkinje cell null mutants gained weight normally (Fig. 3C and D). Further, of 36 *Npc1*$^{flox/-}$*;Pcp2-Cre*$^{+}$ mice generated, none died prematurely, including seven followed for 20 weeks (Fig. 3C and D insets) and a small number followed as long as 40 weeks. In contrast, global null mutants never survived longer than 9 weeks (Fig. 2D). We conclude that Npc1 deficiency in Purkinje cells is sufficient to cause motor impairment but not other features of the disease phenotype in mice.

Cell specific deletion of *Npc1* causes Purkinje cell loss in a spatial and temporal pattern similar to that of global null mice

Following phenotype analysis of Purkinje cell specific null mice, we used histological examination of cerebellar tissue to determine effects on Purkinje cell survival. Sagittal midline cerebellar sections stained for calbindin revealed loss of Purkinje cells by 7 weeks of age, starting in the anterior zone (lobules II–V) and progressing posteriorly (Fig. 4A). This same pattern of Purkinje cell loss has been documented previously in *Npc1* global null mutants (22). Activation and proliferation of microglia and astrocytes were also detected in Purkinje cell null mutants as early as 7 weeks, advancing in a pattern that mirrored Purkinje cell loss (Supplementary Material, Fig. S2). Quantification of Purkinje cells in midline cerebellar sections demonstrated that the rate of loss fit tightly to a model incorporating a plateau followed by exponential decay (Fig. 4B). That cell loss began after a plateau was supported by quantifying Purkinje cells in conditional null mutants and controls at 4 weeks, prior to the onset of exponential loss (Fig. 4C). These data are consistent with a model that a single hit underlies neuronal loss in NPC, and are similar to observations in other neurodegenerative disorders (27).

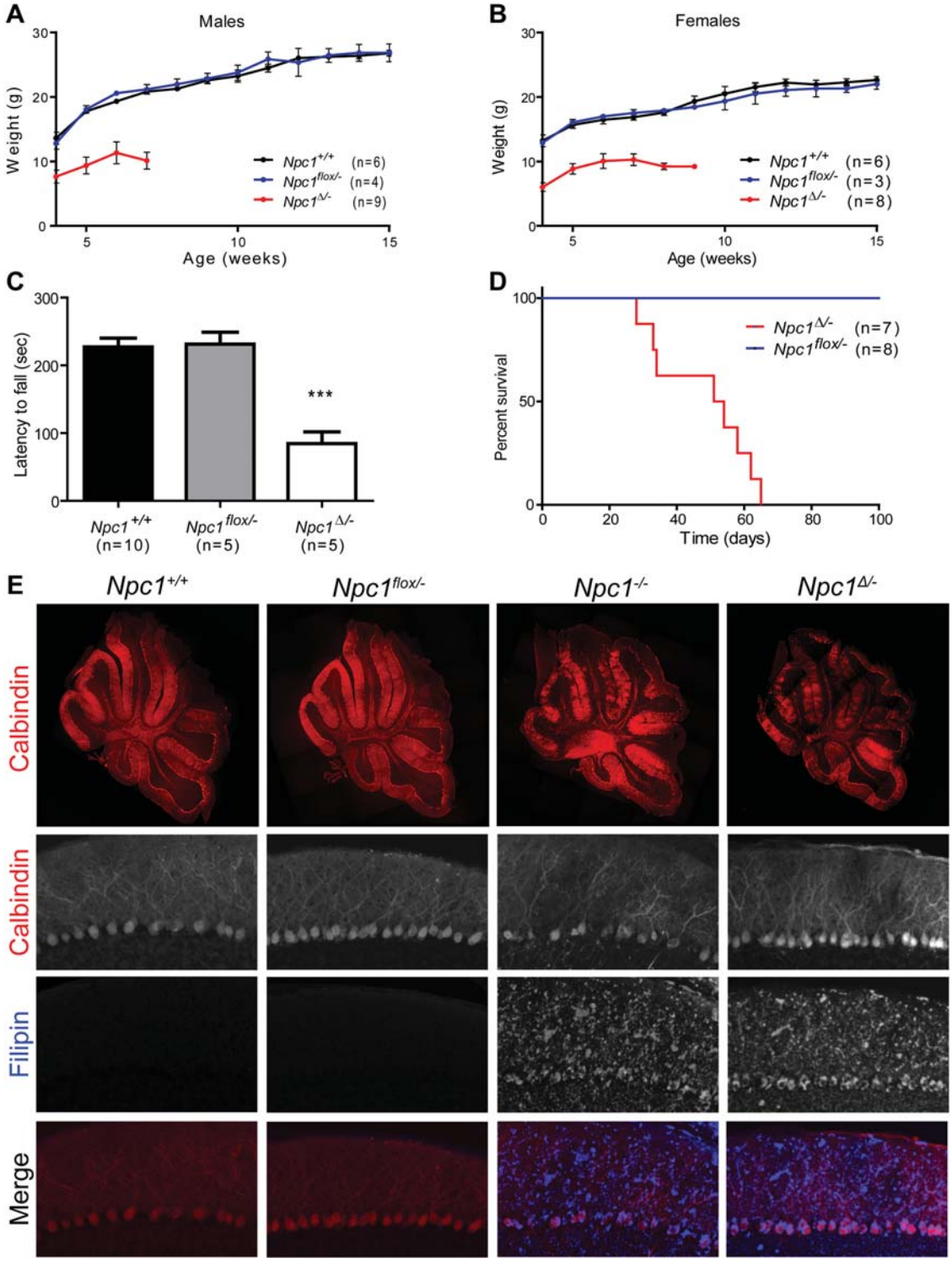

Figure 2. Phenotype and pathology following germline deletion of *Npc*1. (**A**, **B**) Weight curves for male (A) and female (B) mice. (**C**) Rotarod performance at 7 weeks. Data are mean ± SEM. $^{***}P < 0.001$. (**D**) Kaplan–Meyer survival curve. $P = 0.0001$. (**E**) Cerebellar pathology at 7 weeks. Row 1: Calbindin immunofluorescence demonstrates patchy Purkinje cell loss in the anterior zone of the cerebellum in $Npc1^{-/-}$ and $Npc1^{\Delta/-}$ mice. Rows 2–4: Calbindin and filipin co-stain highlight filipin-positive lipid accumulations in $Npc1^{-/-}$ and $Npc1^{\Delta/-}$ cerebellum (Original magnification 100×).

Our findings establish that deletion of *Npc1* only in Purkinje cells is sufficient to cause cell autonomous degeneration. However, we considered the possibility that dysfunction of *Npc1*-null glia may additionally enhance neurodegeneration in NPC disease. If this were the case, it would be expected that Purkinje cell loss would occur more slowly in Purkinje cell specific null mutants than in global null mutants. Ideally, this would be determined by comparing half-lives of

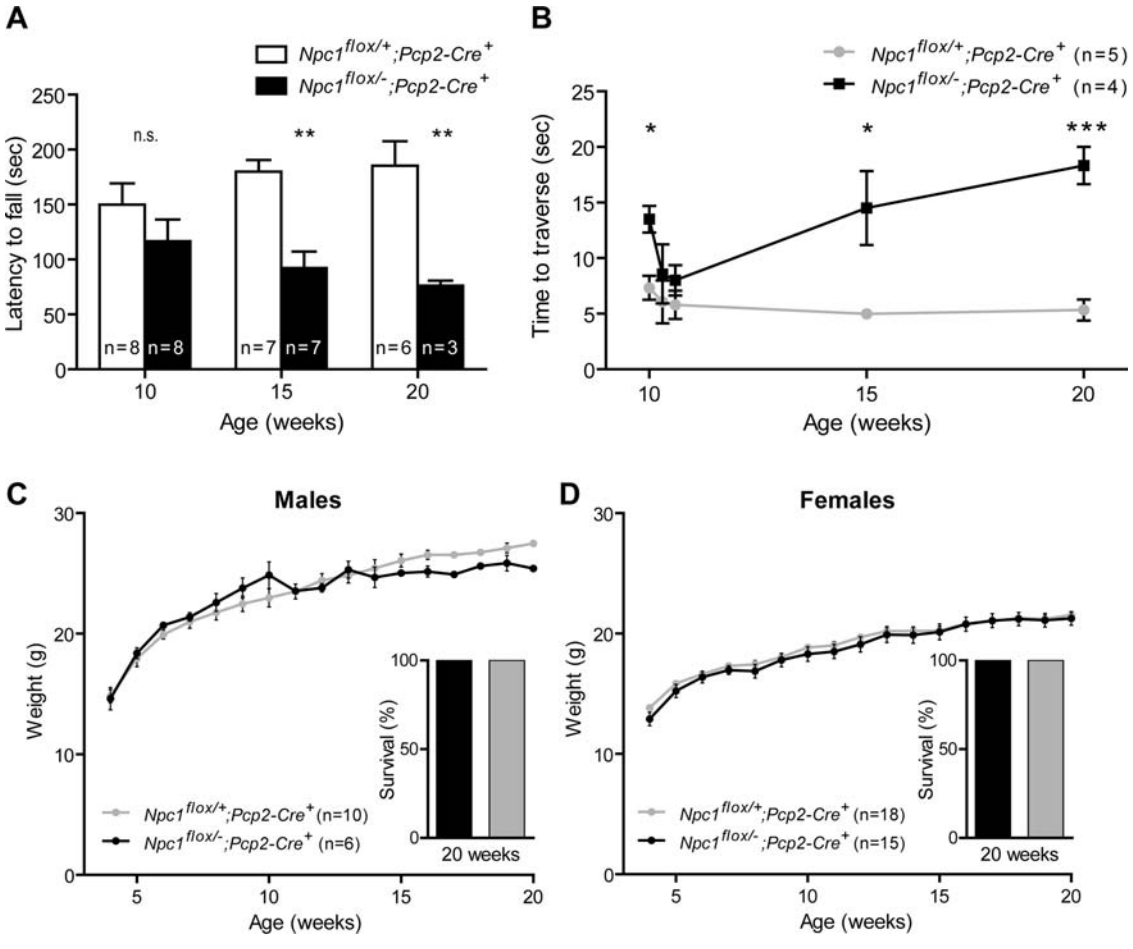

Figure 3. Purkinje cell specific deletion of *Npc1* impairs rotarod and balance beam performance. (**A**, **B**) Age-dependent performance on rotarod (A) and balance beam (B). Data are mean ± SEM. n.s. not significant, $^{*}P < 0.05$, $^{**}P < 0.01$, $^{***}P < 0.001$. (**C**, **D**) Weight curves for male (A) and female (B) mice. Insets depict 100% survival of mice followed for 20 weeks.

Purkinje cells in $Npc1^{flox/-}$;*Pcp2-Cre*$^{+}$ and $Npc1^{\Delta/-}$ mice. However, due to the early death of *Npc1* global null mutants on the C57BL6/J background, we were unable to reliably determine the half life of Purkinje cell loss in these animals. To gain an approximation, we compared the initial rate of Purkinje cell loss in $Npc1^{flox/-}$;*Pcp2-Cre*$^{+}$ and $Npc1^{\Delta/-}$ mice between 5.5 and 7 weeks (Fig. 4C). No significant difference was observed between the slopes of these lines (-2.37 ± 0.98 versus -3.93 ± 2.53, $P = 0.59$). A small, but significant, right-shift of the curve for $Npc1^{flox/-}$;*Pcp2-Cre*$^{+}$ mice was observed, suggesting that the onset of Purkinje cell loss was slightly delayed in these mice, likely owing to the timing of *Npc1* deletion. We conclude that cell death occurs at approximately the same rate regardless of whether *Npc1* is deleted in all cells or only in Purkinje cells, and that the rate is independent of the developmental timing of *Npc1* deletion.

Differential survival of Purkinje cell subpopulations

Our initial analysis suggested that Purkinje cell specific deletion of *Npc1* recapitulated the anterior–posterior gradient of cell loss that has been demonstrated to occur in global null mutants (22). To verify this observation, we quantified Purkinje cell survival by lobule (Fig. 5A), and established that conditional null mutants exhibited this same pattern of cell loss. Aging of $Npc1^{flox/-}$;*Pcp2-Cre*$^{+}$ mice beyond the typical lifespan of $Npc1^{-/-}$ mice, however, allowed a striking observation to emerge. In lobule X, although the anterior-most ∼15% of Purkinje cells were lost by 10 weeks, there was no further cell loss between 10 and 20 weeks. This was in stark contrast with lobules II–V, where Purkinje cell loss was >75% at 10 weeks and approached 100% by 15 weeks. This observation suggested that a marked difference exists between these two ostensibly similar neuronal populations in their susceptibility to cell death following Npc1 deficiency. The resistance of lobule X Purkinje cells was associated with delayed accumulation of unesterified cholesterol as detected by staining with the fluorescent dye filipin (Fig. 5B). Nearly all Purkinje cells in lobules II–V were filipin positive by 4 weeks. In the remainder of the cerebellum, there was roughly ∼60% filipin positivity at this age, progressing to 80–90% by 7 weeks and nearly 100% by 10 weeks. This differential rate of unesterified cholesterol accumulation and Purkinje cell loss was not explained by delayed deletion of *Npc1* exon 9, as crossing *Pcp2-Cre* mice with ROSA reporter mice demonstrated that nearly all Purkinje cells stained for β-galactosidase at 4 weeks (Fig. 5C). Our data

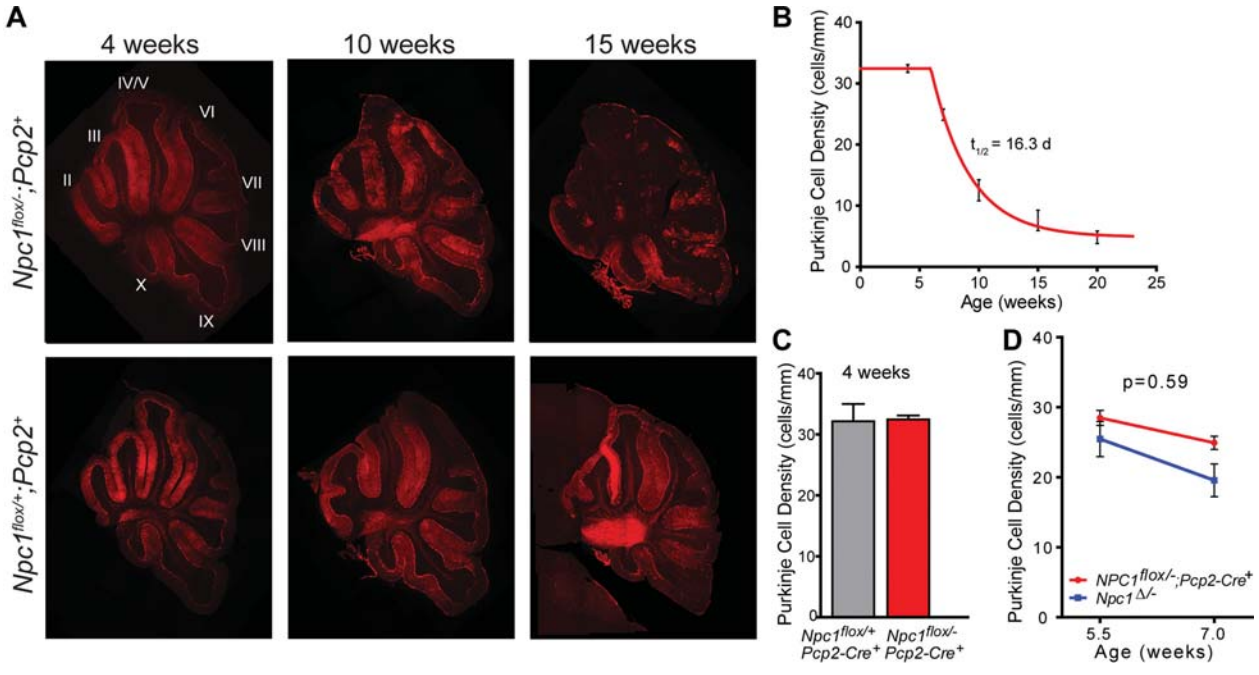

Figure 4. Cell autonomous Purkinje cell loss. (**A**) Calbindin immunofluorescence demonstrates progressive anterior-to-posterior Purkinje cell loss in *Npc1*$^{flox/-}$;*Pcp2-Cre*$^{+}$ mice (top row), but not *Npc1*$^{flox/+}$;*Pcp2-Cre*$^{+}$ controls (bottom row). Roman numerals label cerebellar lobules. (**B**) Quantification of Purkinje cell loss over time in the cerebellar midline, expressed as Purkinje cell density. Slope of the exponential decay phase indicates a half-life for Purkinje cells of 16.3 days. (**C**) Purkinje cell density at 4 weeks, demonstrating no cell loss at this age in *Npc1*$^{flox/-}$;*Pcp2-Cre*$^{+}$ mice versus *Npc1*$^{flox/+}$;*Pcp2-Cre*$^{+}$ controls. (**D**) Initial rate of Purkinje cell loss, calculated from density at 5.5 and 7 weeks, for *Npc1*$^{flox/-}$;*Pcp2-Cre*$^{+}$ mice and *Npc1*$^{\Delta/-}$ global null mice (mean ± SEM).

establish that patterned Purkinje cell loss is a manifestation of cell autonomous toxicity mediated by *Npc1* deletion. Although lobule X Purkinje cells also display delayed cholesterol accumulation, we believe that this is unlikely to be a sufficient explanation of their resistance since they continued to survive long after the acquisition of filipin staining.

Absence of electrophysiological abnormalities in degenerating Purkinje cells

To further investigate the mechanism of neurodegeneration in NPC, we considered the possibility that electrophysiological dysfunction contributed to Purkinje cell death. Ion channel mutations are a known cause of inherited neurodegenerative ataxias in humans and mice (28,29), and channel function is influenced by membrane lipid composition (30), leading to a potential mechanism by which lipid trafficking defects could influence neuronal function. We therefore investigated the extent to which electrophysiological properties differed between vulnerable and resistant Purkinje cell subpopulations. We also sought to determine whether lobule X Purkinje neurons, which appear histologically intact despite the presence of filipin-positive lipid storage material, are able to support normal physiology. Normal Purkinje neurons exhibit characteristic spontaneous repetitive firing (31). The spontaneous firing of these neurons depends on the presence of the correct composition of plasma membrane ion channels and normal cellular energy homeostasis (32). Therefore, assessment of electrophysiological function provided a means to evaluate several pathways that could influence the function and survival of Purkinje cells in NPC mice.

We measured the spontaneous activity of Purkinje cells in acute cerebellar slices from 10-week *Npc1*$^{flox/-}$;*Pcp2-Cre*$^{+}$ mice (Fig. 6). Purkinje cells in lobule X (Fig. 6A), which are resistant to the toxicity of Npc1 deficiency, demonstrated normal spontaneous firing ($n = 5$, not shown), indicating that these cells are both morphologically and electrophysiologically intact at this age. Surviving Purkinje cells in the anterior zone (lobules II–V) were infrequent, and those that remained had shrunken soma and dystrophic dendrites (Fig. 6B). Unexpectedly, these cells also showed normal spontaneous activity as measured by whole-cell recordings ($n = 6$, Fig. 6C). To confirm that supplying energy substrates in the internal solution was not restoring firing in these neurons, we also assessed spontaneous activity through extracellular recordings. Extracellularly recorded spike frequency was similar to recordings obtained in the whole cell mode ($n = 4$, Fig. 6D). The pattern of repetitive firing in lobule II–V neurons was indistinguishable from that of lobule X Purkinje cells. We also determined if the spike width, a measure of potassium current-dependant action potential repolarization (33), differed between Purkinje cells in the anterior and posterior cerebellum. Spike width was indistinguishable between lobule II–V and lobule X neurons (0.37 ± 0.02 and 0.44 ± 0.05, $P = 0.2$, Fig. 6E). Although the surviving lobule II–IV neurons were smaller and had abnormal dendrites, their passive membrane properties including total cellular capacitance were similar to those of lobule X neurons (Fig. 6F). These findings indicate that Purkinje neurons in NPC mice retain plasma membrane integrity even as morphological changes are occurring. Altogether, our observations indicate that electrophysiological dysfunction is unlikely to precede the death of Npc1 deficient Purkinje cells, and

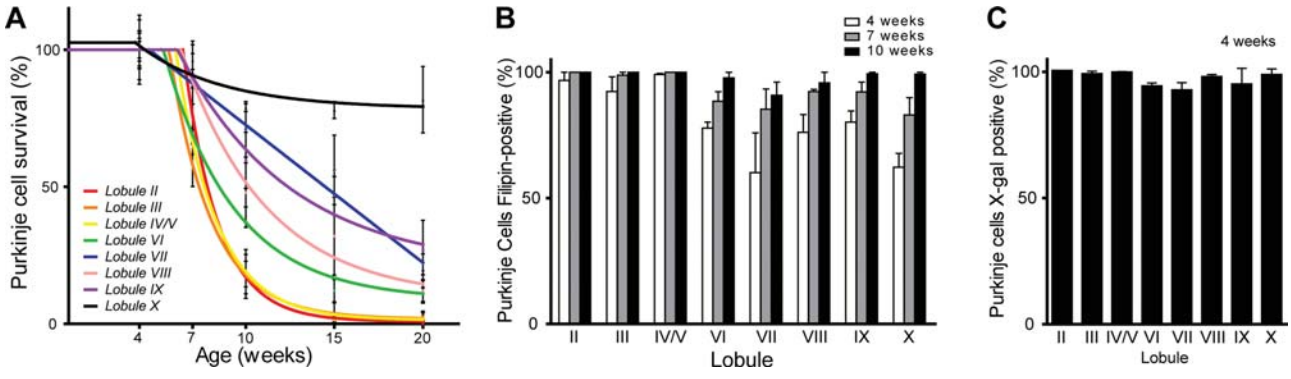

Figure 5. Differential survival of Purkinje cell subpopulations. (**A**) Purkinje cell loss by lobule in midline sections of *Npc1*$^{flox/-}$;*Pcp2-Cre*$^{+}$ mice (mean ± SEM). (**B**) Lipid accumulation in *Npc1*$^{flox/-}$;*Pcp2-Cre*$^{+}$ mice. Calbindin-positive Purkinje cells were scored as filipin-positive or filipin-negative in midline cerebellar sections from mice at 4, 7 and 10 weeks ($n = 3$ mice at each age). Data are mean ± SEM. (**C**) *Pcp2-Cre* expression at 4 weeks, as determined by crossing with ROSA reporter mice. Calbindin-positive Purkinje cells were scored for X-gal staining in midline cerebellar sections. Data are mean ± SEM.

suggest that defects in ion homeostasis and energy metabolism do not underlie the vulnerability of Purkinje cells in the anterior zone of the cerebellum. Further, our data demonstrate that Purkinje cells maintain normal electrophysiological behavior despite NPC-induced lipid trafficking defects.

DISCUSSION

Here, we characterize a conditional null mutant of the mouse *Npc1* gene, and demonstrate that gene deletion restricted to Purkinje cells is sufficient to cause cell autonomous neuronal loss. Purkinje cell specific null mutants display impaired motor function, but not weight loss or early death, indicating that cerebellar degeneration accounts for limited aspects of the NPC phenotype in mice. Our data also establish that Purkinje cells in the anterior cerebellar lobules exhibit vulnerability to the toxicity of Npc1 deficiency, whereas those in the posterior lobules unexpectedly show remarkable resistance. Finally, we demonstrate that Npc1-deficient Purkinje cells in both susceptible and resistant lobules display normal electrophysiological activity prior to their degeneration, indicating that defects in ion homeostasis and energy metabolism do not underlie their loss. Our findings demonstrate that Npc1 deficiency leads to cell autonomous, selective neuronal vulnerability and suggest that the ataxic symptoms of NPC disease arise from Purkinje cell death rather than cellular dysfunction.

Studies of a diverse array of neurodegenerative disorders have yielded increasing evidence that neuronal dysfunction and death can arise from defects extrinsic to the neurons that are lost. Among the most compelling evidence in support of this conclusion comes from studies in animal models. For example, expression of polyglutamine-expanded ataxin-7, the cause of spinocerebellar ataxia type 7, only in Bergmann glia is sufficient to trigger Purkinje cell degeneration in mice (34). Similarly, the deletion of mutant SOD1 from microglia (35) or astrocytes (36) slows disease progression in a mouse model of familial amyotrophic lateral sclerosis. Additionally, studies in a transgenic mouse model of Huntington disease indicate that pathological interactions between neurons are important for cortical pathology (37). These observations and others have lead to a model in which neurodegeneration can be caused by cell autonomous mechanisms, defects in supporting glia, aberrant interactions between neurons or a combination of these (38).

The data reported here establish that Purkinje cell degeneration in NPC mice is cell autonomous. Our findings support conclusions from the analysis of a chimeric mouse model of NPC disease (15), and extend this work by showing the extent of selective vulnerability of Purkinje cell subpopulations. As *Npc1* deletion mediated by the *Pcp2-Cre* transgene occurs in post-developmental Purkinje cells (26), we also conclude that this neuronal loss is independent of events during embryonic or early postnatal development. Prior studies raised the possibility that degeneration of Purkinje cells in NPC mice may arise from developmental defects, perhaps mediated by decreased production of neurosteroids to guide neuronal maturation (20). Our findings do not support this conclusion. Whereas *Npc1* is deleted weeks later in *Npc1*$^{flox/-}$;*Pcp2-Cre*$^{+}$ mice than in *Npc1*$^{\Delta/-}$ mice, the rate of Purkinje cell degeneration is similar in both sets of animals. Cell loss is therefore independent of the cumulative time following *Npc1* deletion, and instead likely reflects a requirement for Npc1 only after Purkinje cells reach maturity.

It is notable that *Npc1*$^{flox/-}$;*Pcp2-Cre*$^{+}$ mice do not exhibit weight loss or early death. Although there has been some speculation that cerebellar ataxia impairs feeding ability of NPC mice, in turn causing weight loss and death, our data are inconsistent with this notion. Prior work established that weight loss and death are due to Npc1 deficiency in the nervous system (10), yet the identity of the specific cellular population(s) responsible for these aspects of the phenotype remains enigmatic. It is possible that weight loss stems from dysfunction of feeding centers in the hypothalamus, and that early death results from degeneration of distinct brain regions required for support life, such as the brainstem (39). Our data suggest that therapies targeted to Purkinje cells would be expected to rescue limited aspects of the neurological phenotype, particularly those reflecting ataxia. Weight loss and early death are likely mediated by impairment of other cell types, and further studies are needed to clarify their identity.

Our observation that Purkinje cells in posterior cerebellar lobules exhibit resistance to the toxicity of Npc1 deficiency prompted us to consider the possibility that

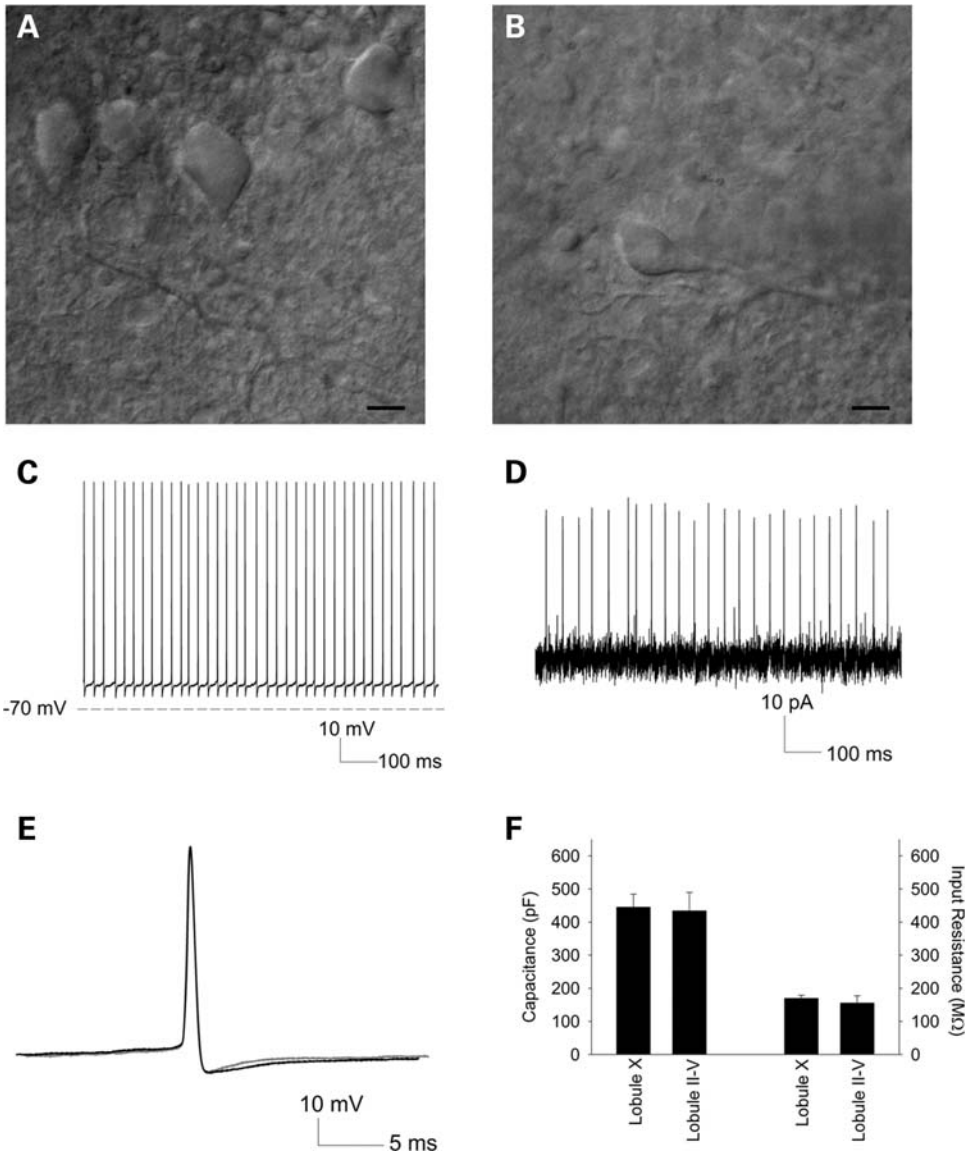

Figure 6. Electrophysiology of Purkinje cell subpopulations. (**A**, **B**) Infrared differential interference contrast (IR-DIC) microscopy of representative Purkinje cells from which recordings were performed, in lobules X (A) and III (B). Scale bar = 10 μM. (**C**) Whole cell recording from a lobule III Purkinje cell. (**D**) Extracellular recording from a lobule IV/V Purkinje cell. (**E**) Overlay of action potentials from a lobule X (black) and lobule III (grey) Purkinje cell. (**F**) Passive membrane properties of anterior zone versus lobule X Purkinje cells, including capacitance (left) and input resistance (right).

electrophysiological dysfunction contributed to the differential survival of Purkinje cell subpopulations in NPC. To test this notion, we examined the spontaneous firing of Purkinje cells in acute cerebellar slices from 10-week $Npc1^{flox/-}$;$Pcp2\text{-}Cre^{+}$ mice. Surprisingly, Purkinje cells from both anterior and posterior cerebellar lobules exhibited normal spontaneous firing activity. These data indicate that electrophysiological defects do not underlie neuronal vulnerability, and that Purkinje cells can function despite the presence of filipin-positive lipid storage material. On the basis of these findings, we suggest that the cerebellar ataxia that develops in these mice is largely dependent upon Purkinje cell death rather than cellular dysfunction. Consistent with this interpretation, $Npc1^{flox/-}$;$Pcp2\text{-}Cre^{+}$ mice develop symptoms only after the loss of a substantial proportion of their Purkinje cells. This is in marked contrast with other cerebellar disorders, including many of the spinocerebellar ataxias, episodic ataxias and paraneoplastic ataxia, wherein symptoms become evident prior to, or even in the absence of, frank Purkinje cell loss (40). This observation raises the possibility that therapies directed at preventing neuron death (41) may be as valuable as those aimed at relieving the primary lipid trafficking defect (21,42) for treating aspects of the neurological symptoms in NPC disease.

MATERIALS AND METHODS

Mice

The targeting vector was constructed using a BAC containing the C57BL/6J *Npc1* genomic clone, which was digested with

BamH1 to obtain a 9.3 kb fragment of the *Npc1* gene that includes exon 9. This fragment was subcloned into pcDNA3, and then digested with Ssp1 and *Eco*RV to generate a 3.0 kb 5′ arm and with Asp718 to generate a 5.2 kb 3′ arm. These arms were cloned into ploxPFlpneo, a vector that contains the neomycin resistance gene and the PGK promoter flanked by *FRT* sites (gift of Dr James Shayman, University of Michigan). Included within the neomycin resistance gene is an *Eco*RV site that was used during screening for recombinants by Southern blot by probing for exons 5 and 18, both of which fall outside the targeting vector. *Npc1* exon 9 and flanking intronic sequence were amplified from C57BL/6J genomic DNA by high fidelity PCR, sequenced, and inserted between *lox*P sites. The targeting vector was electroporated into Bruce4 mouse embryonic stem cells, a line derived from C57BL6 mice that shares 85% genetic identity with this strain (43). Euploid clones that had undergone homologous recombination were injected into albino C57BL6/J blastocysts. Germline transmission of the floxed allele in offspring of two independently derived chimeras was confirmed by the appearance of black fur, Southern blotting and PCR. Resulting mice were crossed with mice expressing FLP recombinase (Jackson Laboratories, #003800, backcrossed to C57BL6/J for 10 generations) to remove the Neo cassette. These offspring were then backcrossed to C57BL6/J for seven generations and interbred to generate floxed homozygotes. *Pcp2-Cre* mice were obtained from Jackson Laboratories (#004146) and backcrossed to C57BL6/J for seven generations. $npc1^{nih}$ mice were obtained from Jackson Laboratories (#003092) and backcrossed to C57BL6/J for 10 generations. $Npc1^{\Delta/+}$ mice were generated by mating $Npc1^{flox/+}$ mice with *EIIa-Cre* mice (Jackson #003724, backcrossed to C57BL/6J for 10 generations) and breeding the resulting mosaics with wild-type C57BL6/J mice. All animal procedures were approved by the University of Michigan Committee on the Use and Care of Animals.

Genotyping

Genotyping was performed on DNA isolated from tail biopsy at the time of weaning. PCR primers for $Npc1^{flox}$ mice were primer 1, 5′- TACTTGGTAGTTGTCAGGTAGGCTTATG CT-3′; primer 2, 5′- GTCCACAGAACGGGTCATCT-3′; and primer 3, 5′- ACACTGCAACGGGCTCCTTTG-3′. PCR was performed for 30 cycles, with denaturation at 95° for 30 s, annealing at 62° for 30 s and extension at 72° for 2 min. Predicted PCR products are demonstrated in Figure 1C. Genotyping of *Cre* mice was as described by Jackson Laboratories.

Western blotting

Liver lysates were homogenized in RIPA buffer (Thermo Scientific) with complete Protease Inhibitor Cocktail (Roche) plus 50 mM sodium fluoride and 5 mM sodium orthovanadate (Sigma). Samples were electrophoresed through a 10% SDS-polyacrylamide gel and transferred to nitrocellulose membranes (BioRad) on a semidry transfer apparatus. Immunoreactivity was detected by Immobilon chemilluminescent substrate (Millipore). Antibodies used were rabbit anti-NPC1 (1:1000, Abcam) and GAPDH (1:20 000 Abcam).

Gene expression analysis

Total RNA was isolated from liver using TRIzol (Invitrogen) per the manufacturer's protocol. cDNA was synthesized using the High Capacity cDNA Archive Kit (Applied Biosystems). Quantitative real time PCR (RT–PCR) was performed on 5 ng cDNA per reaction, in duplicate. Primers and probes for *Npc1* exon 1–2, *Npc1* exon 9–10 and 18S rRNA were purchased from Applied Biosystems. Threshold cycle (Ct) values were determined on an ABI Prism 7900HT Sequence Detection System. Relative expression values were calculated by the standard curve method and normalized to 18S rRNA.

Histology

Mice were anesthetized with isofluorane and perfused transcardially with 0.9% normal saline followed by 4% paraformaldehyde. Brain and liver were removed and post-fixed in 4% paraformaldehyde overnight. Brains were bisected, with the right half processed for paraffin embedding and the left half processed for frozen sections. Prior to freezing, brain tissue was cryoprotected in 30% sucrose for 48 h at 4°C. Brains were frozen in isopentane chilled by dry ice and embedded in OCT (Tissue-Tek). Free floating sections were prepared with a cryostat at 30 μm and used for immunofluorescent staining for calbindin (1:1000, Sigma), using secondary antibodies conjugated to Alexa Fluor 594 (Molecular Probes) for visualization. Sections were subsequently stained for unesterified cholesterol by incubating tissue for 90 min in PBS with 10% fetal bovine serum plus 25 μg/ml filipin (Sigma). Images were captured on a Zeiss Axioplan 2 imaging system. Paraffin-embedded sections were prepared at 5 μm and used for H&E staining, Iba1 (1:5000, Wako) and GFAP (1:1000, Dako) immunohistochemistry. Quantification of Purkinje cell loss was performed on H&E stained sections. Purkinje cells were recognized as large cells with amphophilic cytoplasm, large nuclei with open chromatin and prominent nucleoli that were located in the Purkinje layer. Counts were normalized to the length of the Purkinje layer, as measured by NIH ImageJ software and reported as Purkinje cell density.

Phenotype analysis

All mice were weighed weekly. Motor function was measured by the balance beam and rotarod tests. The balance beam consists of a 5 mm wide square beam suspended at 50 cm. Mice were trained at 10 weeks of age to cross the beam quickly and without stopping. Mice were then tested in triplicate on three consecutive days, followed by retesting at 15 and 20 weeks. Data were reported as time to traverse the beam, allowing a maximum of 20 s and scoring falls as 20 s (44). For rotarod analysis, mice were trained for 5 min on a rod rotating at 5 rpm. Four additional trials were performed on each of 2 days at 1 h intervals on a rod accelerating linearly from 5 to 40 rpm over 5 min. Data reported for each mouse is the average latency to fall from the rod for the four trials on the second day of testing. Clinging to the rod for a full rotation

was scored as a fall. Mice were allowed to stay on the rotarod for a maximum of 5 min. All behavioral tests were performed in the latter half of the light phase of a 12-h light–dark cycle. The endpoint used for survival analysis was when mice appeared moribund according to the guidelines of the University of Michigan Committee on the Use and Care of Animals.

Electrophysiology

Whole-cell recordings were obtained from Purkinje neurons in 300 μm parasagittal cerebellar slices prepared from 10 week old mice. Vibratome sections were cut in ice-cold solution containing (in mM): 87 NaCl, 2.5 KCl, 25 $NaHCO_3$, 1 NaH_2PO_4, 0.5 $CaCl_2$, 7 $MgCl_2$, 75 sucrose and 10 glucose, bubbled with 5% CO_2/95% O_2. Slices were incubated at 33°C in artificial CSF (ACSF) containing (in mM): 125 NaCl, 3.5 KCl, 26 $NaHCO_3$, 1.25 NaH_2PO_4, 2 $CaCl_2$, 1 $MgCl_2$ and 10 glucose, bubbled with 5% CO_2/95% O_2 for 45 min. Purkinje neurons were visualized with infrared differential interference contrast (IR-DIC) optics on a Nikon upright microscope. Borosilicate glass patch pipettes (with resistances of 4–6 MΩ) were filled with internal recording solution containing (in mM): 119 K Gluconate, 2 Na Gluconate, 6 NaCl, 2 $MgCl_2$, 10 EGTA, 10 HEPES, 14 Tris-Phosphocreatine, 4 MgATP, 0.3 tris-GTP. Whole-cell recordings were made in ACSF at room temperature 1–5 h after slice preparation using an Axopatch 200B amplifier, Digidata 1440A interface and pClamp-10 software (Molecular Devices). Voltage data were acquired in the fast current clamp mode of the amplifier and filtered at 2 kHz. The fast current-clamp mode is necessary to reduce distortion of action potentials observed when patch-clamp amplifiers are used in current-clamp mode (45). We could obtain stable recordings without oscillations in fast current-clamp mode with electrode resistances above 3 MΩ, as has been previously reported (46). Series resistance was monitored but not compensated; cells were rejected if the series resistance exceeded 20 MΩ. Total cell capacitance was calculated from measurement of the area under current transients evoked from a 10 mV depolarizing step from −80 mV. Input resistance was calculated from the change in the leak current from an applied 10 mV voltage step from −80 mV. Data were digitized at >10 kHz. Voltage traces were corrected for a 10 mV liquid junction potential.

Statistics

Statistical significance was assessed by unpaired Student's *t* test (for comparison of two means) or ANOVA (for comparison of more than two mean). The Newman–Keuls *post hoc* test was performed to carry out pairwise comparisons of group means if ANOVA rejected the null hypothesis. Statistics were performed using the software package Prism 4 (GraphPad Software). *P*-values less than 0.05 were considered significant.

SUPPLEMENTARY MATERIAL

Supplementary Material is available at *HMG* online.

ACKNOWLEDGEMENTS

We thank Dr Roger Albin for advice on Purkinje cell quantification and Dr Miriam Meisler for comments on our manuscript.

Conflict of Interest statement. None declared.

FUNDING

This work was supported by grants from the National Institutes of Health (R01 NS063967 and R03 NS057150 to A.P.L., F31 NS51143 to C.D.P. and T32 GM07863 and T32 MH014279 to M.J.E.) and the Fauver Family Fund (to V.G.S. and H.L.P.).

REFERENCES

1. Higgins, J.J., Patterson, M.C., Dambrosia, J.M., Pikus, A.T., Pentchev, P.G., Sato, S., Brady, R.O. and Barton, N.W. (1992) A clinical staging classification for type C Niemann-Pick disease. *Neurology*, **42**, 2286–2290.
2. Carstea, E.D., Morris, J.A., Coleman, K.G., Loftus, S.K., Zhang, D., Cummings, C., Gu, J., Rosenfeld, M.A., Pavan, W.J., Krizman, D.B. *et al.* (1997) Niemann-Pick C1 disease gene: homology to mediators of cholesterol homeostasis. *Science*, **277**, 228–231.
3. Naureckiene, S., Sleat, D.E., Lackland, H., Fensom, A., Vanier, M.T., Wattiaux, R., Jadot, M. and Lobel, P. (2000) Identification of HE1 as the second gene of Niemann-Pick C disease. *Science*, **290**, 2298–2301.
4. Kwon, H.J., Abi-Mosleh, L., Wang, M.L., Deisenhofer, J., Goldstein, J.L., Brown, M.S. and Infante, R.E. (2009) Structure of N-terminal domain of NPC1 reveals distinct subdomains for binding and transfer of cholesterol. *Cell*, **137**, 1213–1224.
5. Vanier, M.T. and Millat, G. (2003) Niemann-Pick disease type C. *Clin. Genet.*, **64**, 269–281.
6. Loftus, S.K., Morris, J.A., Carstea, E.D., Gu, J.Z., Cummings, C., Brown, A., Ellison, J., Ohno, K., Rosenfeld, M.A., Tagle, D.A., Pentchev, P.G. and Pavan, W.J. (1997) Murine model of Niemann-Pick C disease: mutation in a cholesterol homeostasis gene. *Science*, **277**, 232–235.
7. Pacheco, C.D. and Lieberman, A.P. (2008) The pathogenesis of Niemann-Pick type C disease: a role for autophagy? *Expert. Rev. Mol. Med.*, **10**, e26.
8. Paul, C.A., Boegle, A.K. and Maue, R.A. (2004) Before the loss: neuronal dysfunction in Niemann-Pick Type C disease. *Biochim. Biophys. Acta.*, **1685**, 63–76.
9. Morris, M.D., Bhuvaneswaran, C., Shio, H. and Fowler, S. (1982) Lysosome lipid storage disorder in NCTR-BALB/c mice. I. Description of the disease and genetics. *Am. J. Pathol.*, **108**, 140–149.
10. Loftus, S.K., Erickson, R.P., Walkley, S.U., Bryant, M.A., Incao, A., Heidenreich, R.A. and Pavan, W.J. (2002) Rescue of neurodegeneration in Niemann-Pick C mice by a prion-promoter-driven Npc1 cDNA transgene. *Hum. Mol. Genet.*, **11**, 3107–3114.
11. Walkley, S.U. (1995) Pyramidal neurons with ectopic dendrites in storage diseases exhibit increased GM2 ganglioside immunoreactivity. *Neuroscience*, **68**, 1027–1035.
12. Auer, I.A., Schmidt, M.L., Lee, V.M., Curry, B., Suzuki, K., Shin, R.W., Pentchev, P.G., Carstea, E.D. and Trojanowski, J.Q. (1995) Paired helical filament tau (PHFtau) in Niemann-Pick type C disease is similar to PHFtau in Alzheimer's disease. *Acta. Neuropathol.*, **90**, 547–551.
13. Bu, B., Li, J., Davies, P. and Vincent, I. (2002) Deregulation of cdk5, hyperphosphorylation, and cytoskeletal pathology in the Niemann-Pick type C murine model. *J. Neurosci.*, **22**, 6515–6525.
14. Lloyd-Evans, E., Morgan, A.J., He, X., Smith, D.A., Elliot-Smith, E., Sillence, D.J., Churchill, G.C., Schuchman, E.H., Galione, A. and Platt, F.M. (2008) Niemann-Pick disease type C1 is a sphingosine storage disease that causes deregulation of lysosomal calcium. *Nat. Med.*, **14**, 1247–1255.
15. Ko, D.C., Milenkovic, L., Beier, S.M., Manuel, H., Buchanan, J. and Scott, M.P. (2005) Cell-autonomous death of cerebellar purkinje

neurons with autophagy in Niemann-Pick type C disease. *PLoS Genet.*, **1**, 81–95.
16. Pacheco, C.D. and Lieberman, A.P. (2007) Lipid trafficking defects increase Beclin-1 and activate autophagy in Niemann-Pick type C disease. *Autophagy*, **3**, 487–489.
17. Phillips, S.E., Woodruff, E.A. 3rd, Liang, P., Patten, M. and Broadie, K. (2008) Neuronal loss of Drosophila NPC1a causes cholesterol aggregation and age-progressive neurodegeneration. *J. Neurosci.*, **28**, 6569–6582.
18. Zhang, M., Strnatka, D., Donohue, C., Hallows, J.L., Vincent, I. and Erickson, R.P. (2008) Astrocyte-only Npc1 reduces neuronal cholesterol and triples life span of Npc1 −/− mice. *J. Neurosci. Res.*, **86**, 2848–2856.
19. Chen, G., Li, H.M., Chen, Y.R., Gu, X.S. and Duan, S. (2007) Decreased estradiol release from astrocytes contributes to the neurodegeneration in a mouse model of Niemann-Pick disease type C. *Glia*, **55**, 1509–1518.
20. Griffin, L.D., Gong, W., Verot, L. and Mellon, S.H. (2004) Niemann-Pick type C disease involves disrupted neurosteroidogenesis and responds to allopregnanolone. *Nat. Med.*, **10**, 704–711.
21. Liu, B., Turley, S.D., Burns, D.K., Miller, A.M., Repa, J.J. and Dietschy, J.M. (2009) Reversal of defective lysosomal transport in NPC disease ameliorates liver dysfunction and neurodegeneration in the npc1 −/− mouse. *Proc. Natl. Acad. Sci. USA*, **106**, 2377–2382.
22. Sarna, J.R., Larouche, M., Marzban, H., Sillitoe, R.V., Rancourt, D.E. and Hawkes, R. (2003) Patterned Purkinje cell degeneration in mouse models of Niemann-Pick type C disease. *J. Comp. Neurol.*, **456**, 279–291.
23. Lakso, M., Pichel, J.G., Gorman, J.R., Sauer, B., Okamoto, Y., Lee, E., Alt, F.W. and Westphal, H. (1996) Efficient *in vivo* manipulation of mouse genomic sequences at the zygote stage. *Proc. Natl. Acad. Sci. USA*, **93**, 5860–5865.
24. Voikar, V., Rauvala, H. and Ikonen, E. (2002) Cognitive deficit and development of motor impairment in a mouse model of Niemann-Pick type C disease. *Behav. Brain Res.*, **132**, 1–10.
25. Liu, B., Li, H., Repa, J.J., Turley, S.D. and Dietschy, J.M. (2008) Genetic variations and treatments that affect the lifespan of the NPC1 mouse. *J. Lipid Res.*, **49**, 663–669.
26. Barski, J.J., Dethleffsen, K. and Meyer, M. (2000) Cre recombinase expression in cerebellar Purkinje cells. *Genesis*, **28**, 93–98.
27. Clarke, G., Collins, R.A., Leavitt, B.R., Andrews, D.F., Hayden, M.R., Lumsden, C.J. and McInnes, R.R. (2000) A one-hit model of cell death in inherited neuronal degenerations. *Nature*, **406**, 195–199.
28. Trudeau, M.M., Dalton, J.C., Day, J.W., Ranum, L.P. and Meisler, M.H. (2006) Heterozygosity for a protein truncation mutation of sodium channel SCN8A in a patient with cerebellar atrophy, ataxia, and mental retardation. *J. Med. Genet.*, **43**, 527–530.
29. Zhuchenko, O., Bailey, J., Bonnen, P., Ashizawa, T., Stockton, D.W., Amos, C., Dobyns, W.B., Subramony, S.H., Zoghbi, H.Y. and Lee, C.C. (1997) Autosomal dominant cerebellar ataxia (SCA6) associated with small polyglutamine expansions in the alpha 1A-voltage-dependent calcium channel. *Nat. Genet.*, **15**, 62–69.
30. Tillman, T.S. and Cascio, M. (2003) Effects of membrane lipids on ion channel structure and function. *Cell. Biochem. Biophys.*, **38**, 161–190.
31. Raman, I.M. and Bean, B.P. (1999) Ionic currents underlying spontaneous action potentials in isolated cerebellar Purkinje neurons. *J. Neurosci.*, **19**, 1663–1674.
32. Genet, S. and Kado, R.T. (1997) Hyperpolarizing current of the Na/K ATPase contributes to the membrane polarization of the Purkinje cell in rat cerebellum. *Pflugers Arch.*, **434**, 559–567.
33. McMahon, A., Fowler, S.C., Perney, T.M., Akemann, W., Knopfel, T. and Joho, R.H. (2004) Allele-dependent changes of olivocerebellar circuit properties in the absence of the voltage-gated potassium channels Kv3.1 and Kv3.3. *Eur. J. Neurosci.*, **19**, 3317–3327.
34. Custer, S.K., Garden, G.A., Gill, N., Rueb, U., Libby, R.T., Schultz, C., Guyenet, S.J., Deller, T., Westrum, L.E., Sopher, B.L. and La Spada, A.R. (2006) Bergmann glia expression of polyglutamine-expanded ataxin-7 produces neurodegeneration by impairing glutamate transport. *Nat. Neurosci.*, **9**, 1302–1311.
35. Boillee, S., Yamanaka, K., Lobsiger, C.S., Copeland, N.G., Jenkins, N.A., Kassiotis, G., Kollias, G. and Cleveland, D.W. (2006) Onset and progression in inherited ALS determined by motor neurons and microglia. *Science*, **312**, 1389–1392.
36. Yamanaka, K., Chun, S.J., Boillee, S., Fujimori-Tonou, N., Yamashita, H., Gutmann, D.H., Takahashi, R., Misawa, H. and Cleveland, D.W. (2008) Astrocytes as determinants of disease progression in inherited amyotrophic lateral sclerosis. *Nat. Neurosci.*, **11**, 251–253.
37. Gu, X., Li, C., Wei, W., Lo, V., Gong, S., Li, S.H., Iwasato, T., Itohara, S., Li, X.J., Mody, I., Heintz, N. and Yang, X.W. (2005) Pathological cell-cell interactions elicited by a neuropathogenic form of mutant Huntingtin contribute to cortical pathogenesis in HD mice. *Neuron*, **46**, 433–444.
38. Lobsiger, C.S. and Cleveland, D.W. (2007) Glial cells as intrinsic components of non-cell-autonomous neurodegenerative disease. *Nat. Neurosci.*, **10**, 1355–1360.
39. Luan, Z., Saito, Y., Miyata, H., Ohama, E., Ninomiya, H. and Ohno, K. (2008) Brainstem neuropathology in a mouse model of Niemann-Pick disease type C. *J. Neurol. Sci.*, **268**, 108–116.
40. Shakkottai, V.G. and Paulson, H.L. (2009) Physiologic alterations in ataxia: channeling changes into novel therapies. *Arch. Neurol.*, **66**, 1196–1201.
41. Alvarez, A.R., Klein, A., Castro, J., Cancino, G.I., Amigo, J., Mosqueira, M., Vargas, L.M., Yevenes, L.F., Bronfman, F.C. and Zanlungo, S. (2008) Imatinib therapy blocks cerebellar apoptosis and improves neurological symptoms in a mouse model of Niemann-Pick type C disease. *FASEB J.*, **22**, 3617–3627.
42. Davidson, C.D., Ali, N.F., Micsenyi, M.C., Stephney, G., Renault, S., Dobrenis, K., Ory, D.S., Vanier, M.T. and Walkley, S.U. (2009) Chronic cyclodextrin treatment of murine Niemann-Pick C disease ameliorates neuronal cholesterol and glycosphingolipid storage and disease progression. *PLoS One*, **4**, e6951.
43. Hughes, E.D., Qu, Y.Y., Genik, S.J., Lyons, R.H., Pacheco, C.D., Lieberman, A.P., Samuelson, L.C., Nasonkin, I.O., Camper, S.A., Van Keuren, M.L. and Saunders, T.L. (2007) Genetic variation in C57BL/6 ES cell lines and genetic instability in the Bruce4 C57BL/6 ES cell line. *Mamm. Genome*, **18**, 549–558.
44. Heng, M.Y., Tallaksen-Greene, S.J., Detloff, P.J. and Albin, R.L. (2007) Longitudinal evaluation of the Hdh(CAG)150 knock-in murine model of Huntington's disease. *J. Neurosci.*, **27**, 8989–8998.
45. Magistretti, J., Mantegazza, M., Guatteo, E. and Wanke, E. (1996) Action potentials recorded with patch-clamp amplifiers: are they genuine? *Trends Neurosci.*, **19**, 530–534.
46. Swensen, A.M. and Bean, B.P. (2003) Ionic mechanisms of burst firing in dissociated Purkinje neurons. *J. Neurosci.*, **23**, 9650–9663.